A Scalable Synthesis of Adjuvanting Antigen Depots Based on Metal-Organic Frameworks

Ryanne N. Ehrman[†a], Olivia R. Brohlin[†a], Yalini H. Wijesundara[a], Sneha Kumari[a], Ikeda Trashi[a], Orikeda Trashi[a], Thomas S. Howlett[a], Fabian C. Herbert[a], Arun Raja[a], Shailendra Koirala[a], Nancy Tran[a], Noora M. Al-Kharji[a], Laurel M. Hagge[a], and Jeremiah J. Gassensmith*[a,b]

[a] Department of Chemistry and Biochemistry, The University of Texas at Dallas, 800 West Campbell Rd., Richardson, TX 75080, USA [b] Department of Biomedical Engineering, The University of Texas at Dallas, 800 West Campbell Rd., Richardson, TX 75080, USA.

KEYWORDS: ZIF-8 encapsulation, MOF degradation analysis, biomimetic mineralization, immune response enhancement

ABSTRACT: Vaccines have saved countless lives by preventing and even irradicating infectious diseases. Commonly used subunit vaccines comprising one or multiple recombinant proteins isolated from a pathogen demonstrate a better safety profile than live or attenuated vaccines. However, the immunogenicity of these vaccines is weak, and therefore, subunit vaccines require a series of doses to achieve sufficient immunity against the pathogen. Here, we show that the biomimetic mineralization of the inert model antigen, ovalbumin (**OVA**), in zeolitic imidazolate framework-8 (**ZIF-8**) significantly improves the humoral immune response over three bolus doses of OVA (**OVA 3×**). Encapsulation of OVA in ZIF-8 (**OVA@ZIF**) demonstrated higher serum antibody titers against OVA than OVA 3×. OVA@ZIF vaccinated mice displayed higher populations of germinal center (**GC**) B cells and IgG1+ GC B cells as opposed to OVA 3×, indicative of class-switching recombination. We show that the mechanism of this phenomenon is at least partly owed to the sustained release of OVA from the ZIF-8 composite, acting as an antigen reservoir for antigen-presenting cells to traffic into the draining lymph node, enhancing the humoral response. Lastly, our model system OVA@ZIF is produced quickly at the gram scale in a laboratory setting, sufficient for up to 20,000 vaccine doses.

Introduction

Edward Jenner discovered that the administration of cowpox blister fluid, which contained live cowpox virus, effectively prevented smallpox; these efforts established the modern field of vaccination and significantly reduced infectious disease-related mortality.[1, 2, 3] Over time, vaccine formulations have evolved, with subunit vaccines emerging as a preferred option, owing to their enhanced safety profile compared to early formulations such as inactivated and live vaccines.[4, 5] Subunit vaccines comprise one or more proteins called antigens (**Ag**) isolated from a specific pathogen.[6] However, these proteinaceous subunit vaccines—like most biomacromolecule-based drugs—are delicate and easily destroyed by environmental factors, requiring cold-chain transportation.[7-9] Additionally, they are often weakly immunogenic and need several doses—typically called boosters—to achieve and maintain complete immunity against the pathogen.[10-13] To achieve high antibody titers and immune memory, many of today's modern vaccines require a prime-boost regimen, where one or more additional doses of vaccine are needed, even in formulations that use adjuvants.[12, 14] However, patient compliance decreases with the number of doses required.[15] The distaste for needles and vaccine side effects deters patients from receiving additional doses, taking a significant toll on the idea of herd immunity.[16-20] Recent work

has shown that sustained release of an antigen from an injected "depot" over several days provokes a more robust immune response than repeat injections. This suggests that a continuous release of Ag from an injection should outperform several injections, thereby removing the need for follow-up doses.

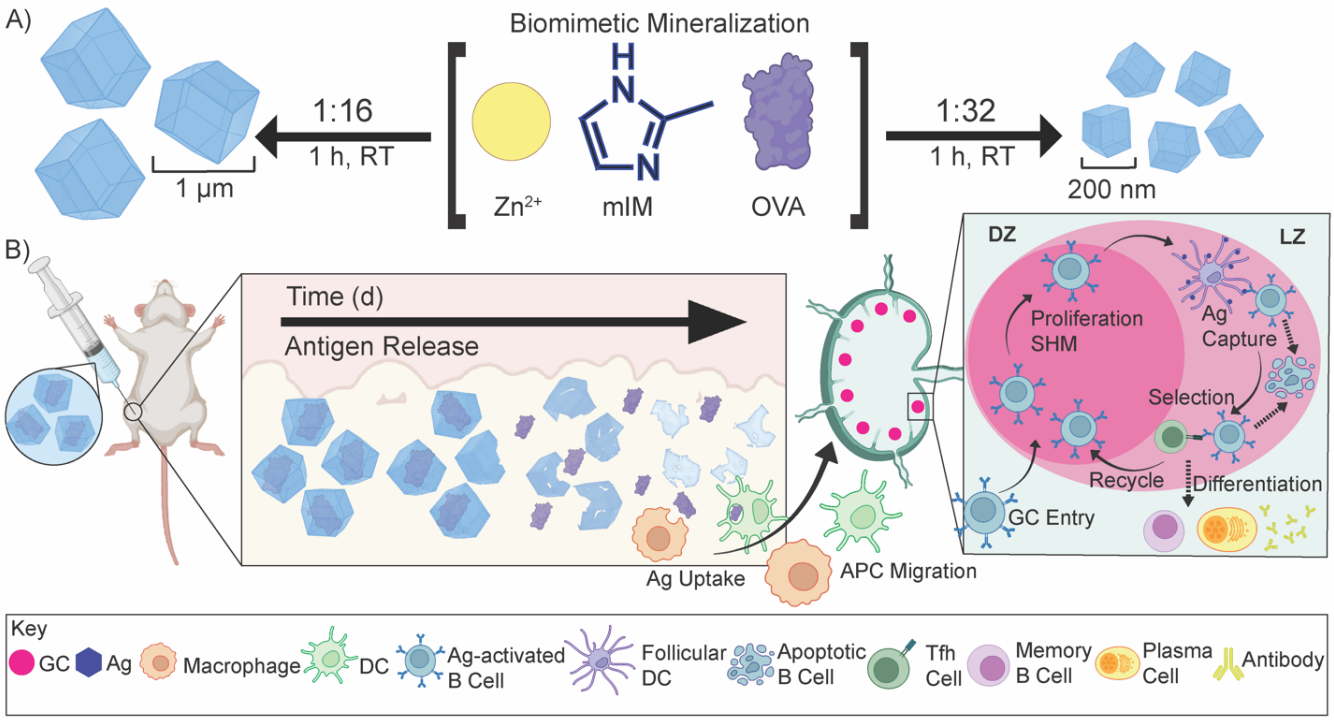

Scheme 1: Biomimetic mineralization of OVA@ZIF and sustained release of antigens. **A)** Synthetic scheme of μ-OVA@ZIF and n-OVA@ZIF. In a "one pot" reaction, Zn^{2+}, mIM, and ovalbumin are suspended in water and react for 1 h at room temperature. By adjusting the ligand-to-metal ratio, we can tune the size of these ZIFs. We formulated a 1:16, micron-sized (~1 μm) and 1:32 nano-sized (~200 nm) μ-OVA@ZIF and n-OVA@ZIF, respectively. **B)** Sustained release of antigens following vaccination, allowing for the formation of GCs. The ZIF-8 crystals slowly degrade in the body, exposing the antigen to the immune system and allowing for a constant supply of antigen to the GC.

The emergence of biomimetic mineralization of delicate biomaterials in a metal-organic framework (**MOF**) has allowed for the development of thermally and enzymatically protected biological material from numerous stressors.[21-26] Recent work has shown that the biofriendly zeolitic imidazolate framework-8 (**ZIF-8**)-encapsulated vaccines promote a more robust immune response against viral nanoparticles or whole-cell bacteria when injected subcutaneously.[21, 22, 27-29] These results are striking but in all cases, the vaccines used have been "self-adjuvanting" as the RNA

or DNA within a virus or the lipopolysaccharides on the inactivated bacteria can induce their own strong immune response. Further, it is not clear what happens to the ZIF inside the skin, nor has size dependence on the toxicity of the particles *in vivo* been assessed as they reside for so long within the tissue.

This work details the MOF encapsulation of a model antigen, ovalbumin (**OVA**), in ZIF-8 (**OVA@ZIF**). By adjusting the metal-to-ligand ratio, we can adjust the size of our vaccine composites. We formulated nano- and micro-sized OVA@ZIF (**n-OVA@ZIF**) and (**μ-OVA@ZIF**), respectively (**Scheme 1A**). We show the process of MOF shell degradation within tissue over several days, which provides a constant supply of antigens to the immune system.[30-32] This provokes a stronger immune response over bolus vaccine.[33] Constant supply of antigen through the depot effect promotes the formation of more developed germinal centers (**GCs — Scheme 1B**) within follicular lymph nodes[34-40] GCs are the location of B cell development, which is crucial for a strong and protective antibody response. We show that Ag release from the ZIF depot promotes GC development and that a single injection of OVA@ZIF produces more antibodies than three injections of OVA (**OVA 3×**). Finally, we show that the synthesis of OVA@ZIF is easily scaled in the laboratory to multi-gram quantities.

Results and Discussion

Synthesis and Cytotoxicity

In a one-pot water synthesis, OVA, 2-methyl imidazole (**mIM**), and Zn^{2+} react at room temperature for 1 h to form the OVA@ZIF composite through biomimetic mineralization. By adjusting the ligand-to-metal ratios, we synthesized two formulations of OVA@ZIF. 1:32 metal-to-ligand ratio yielded nano-sized particles approximately 200 nm in diameter n-OVA@ZIF, and a 1:16 metal-to-ligand ratio yielded micron-sized, approximately 1 μm μ-OVA@ZIF. Scanning electron microscopy (**SEM**) micrographs of both μ-OVA@ZIF and n-OVA@ZIF show approximately 1 μm and 200 nm crystals, respectively (**Figure 1A and 1B**). Powder x-ray diffraction (**PXRD**) spectra confirm the crystallinity of both ZIF-8 formulations and the vaccine formulations μ-OVA@ZIF and n-OVA@ZIF (**Figure 1C**). To help visualize release kinetics and study uptake via flow cytometry, cyanine-7 (**Cy7**) labeled OVA (**OVA[Cy7]**) were produced and encapsulated in both micro-sized (**μ-OVA[Cy7]@ZIF**) and nano-sized (**n-OVA[Cy7]@ZIF**) formulations using the previously mentioned formula. We used the fluorescence of the resulting supernatant to determine encapsulation efficiency (**Figure 1D**). The encapsulation efficiency of both formulations was greater than 98%. μ-OVA[Cy7]@ZIF and n-OVA[Cy7]@ZIF crystals were imaged through confocal laser scanning microscopy (**CLSM**) to confirm that the fluorescence is due to the presence of OVA[Cy7]. CLSM images of non-labeled μ- and n-OVA@ZIF further confirm that the fluorescent intensity is from fluorophore-conjugated protein (**Figure S1**).

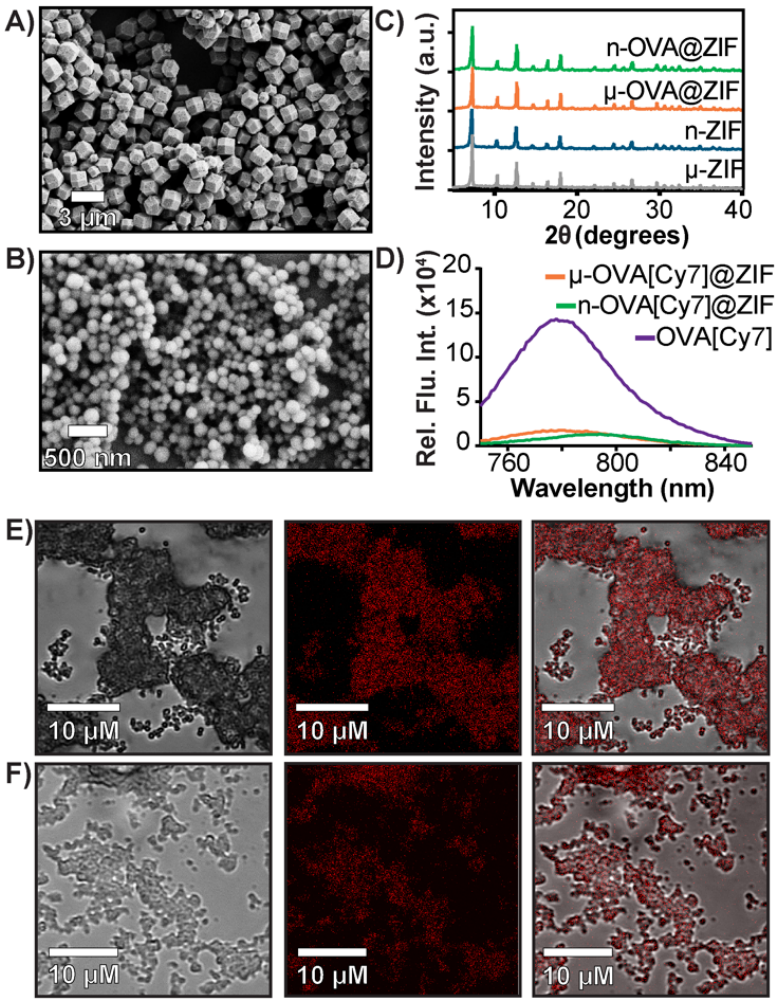

Figure 1. Characterization of OVA@ZIF. **A)** SEM images of µ-OVA@ZIF and **B)** n-OVA@ZIF. **C)** PXRD spectra of OVA@ZIF composites. **D)** Encapsulation efficiency of µ-OVA[Cy7]@ZIF and n-OVA[Cy7]@ZIF as measured by Cy7 fluorescence in the supernatant (λ_{ex}=756 nm and λ_{em}=779 nm). **E)** CLSM images of µ-OVA[Cy7]@ZIF and **F)** n-OVA[Cy7]@ZIF. Brightfield images are shown on the left, fluorescent in the middle, and merged channels on the right.

The safety and toxicology of ZIF-8 have been an area of substantial research;[41-43] however, to the best of our knowledge, it has yet to be benchmarked against current FDA-approved therapeutics. To that end, we conducted a study to compare ZIF-8 formulations against the adjuvant alum, which is nearing a century of use in vaccine formulations.[44] The alum formulations that are typically used to adjuvant an immune response in humans consist of either aluminum hydroxide (**alum(OH)**) or aluminum phosphate (**alum(PO_4)**).[45] We conducted *in vitro* cytotoxicity comparisons between alum salts and our ZIF-8 formulations using lactate dehydrogenase (**LDH**) assay to assess the safety profiles. We utilized immortalized murine RAW 264.7 macrophages (**Fig 2A**) as a standard lab-strain and primary bone marrow-derived macrophages (**BMDMs**) (**Fig 2B**) to represent more realistic toxicities in fresh primary cells. Remarkably, alum(OH) exhibited

significant toxicity in both cell assays, while alum(PO_4) demonstrated higher toxicity in the BMDM assay than in the RAW 264.7 assay. Conversely, the μ-OVA@ZIF formulation showed no toxicity in either cell assay at tested concentrations, while n-OVA@ZIF displayed reduced cell viability in the RAW 264.7 assay without significant cytotoxicity in primary BMDMs. Overall, our results indicate that alum salts have a stronger toxic profile than our μ-OVA@ZIF formulation and are at least comparable with n-OVA@ZIF. This aligns with existing literature,[46, 47] and our study provides evidence that ZIF-8 is a less toxic adjuvant than the FDA-approved alum. Thus, our findings establish that μ-OVA@ZIF is the least toxic among all tested materials. In addition, we assessed cellular uptake using flow cytometry in RAW 264.7 macrophages and found greater uptake of μ-OVA[Cy7]@ZIF compared to n-OVA[Cy7]@ZIF, indicating enhanced cellular uptake for both formulations compared to OVA[Cy7].

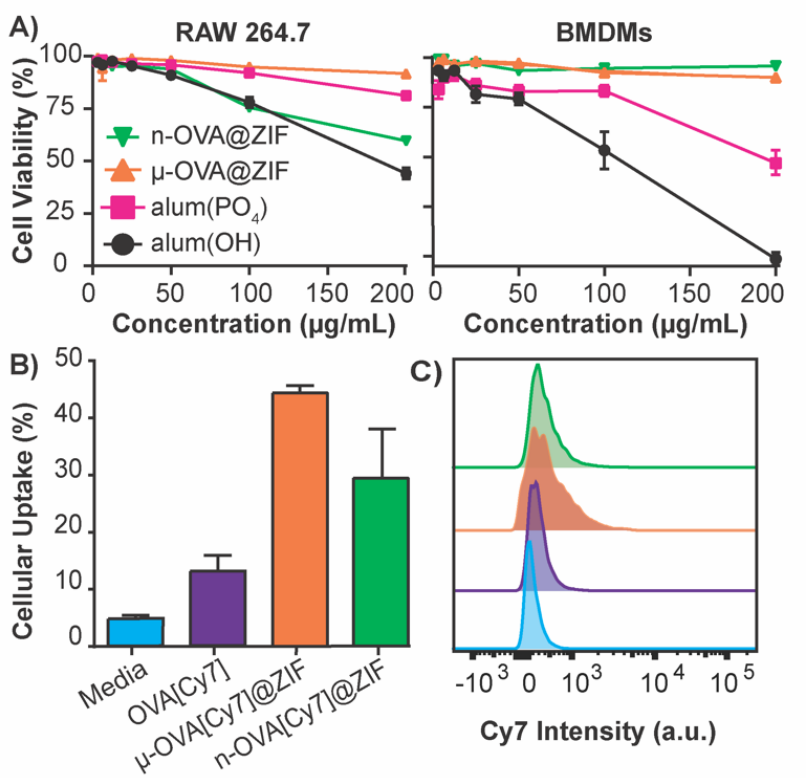

Figure 2. *In vitro* studies of OVA@ZIF. **A)** Cell viability after 4 h incubation of ZIFs and alum in immortalized RAW 264.7 cells (left) and primary BMDMs (right) using LDH assay. **B)** Flow cytometry analysis of the cellular uptake of μ-OVA[Cy7]@ZIF and n-OVA[Cy7]@ZIF by RAW 264.7 macrophage following 4 h incubation. **C)** Representative histogram overlay of flow cytometry plot illustrating the Cy7 intensity of RAW 264.7 macrophages following uptake experiment.

Tissue Residency and Time-Dependent Dissolution

To assess the tissue residency of our formulations, μ-OVA[Cy7]@ZIF, n-OVA[Cy7]@ZIF, and OVA[Cy7] (10 μg of OVA[Cy7]) were subcutaneously injected into the right flank of female

BALB/c mice (n=4), and Cy7 fluorescence intensity was monitored over time through fluorescent live animal imaging (**Figure 3A and B**). Fluorescence intensity diminished in the OVA[Cy7] cohort after 36 h. Whereas μ- and n-OVA[Cy7]@ZIF cohorts demonstrated a significantly longer tissue residency of Ag, with notable fluorescent signal until day 28 and 31, respectively. In agreement with our hypothesis, OVA@ZIF shows significant enhancement of tissue residency of the Ag. However, the n-OVA[Cy7]@ZIF injected mice developed inflammation and skin irritation at the injection site (**Figure S2**). In contrast, the μ-OVA[Cy7]@ZIF formulation showed no signs of *in vivo* toxicity and demonstrated a sustained release profile similar to the n-OVA[Cy7]@ZIF. We extracted the inguinal lymph node (**ILN**) closest to the injection site and the contralateral inguinal lymph node (**CILN**) on 14 d following this single dose of OVA, n-OVA@ZIF, and μ-OVA@ZIF. Saline was used as a negative control. Because of their relative distance from the injection site, both μ-OVA@ZIF and n-OVA@ZIF should have significantly larger draining lymph nodes than the contralateral lymph nodes. Therefore, antigen-mediated trafficking will be higher in the ILN.[48, 49] Gross pathological examination found that μ-OVA@ZIF formulation produced the largest ILN, indicating that this formulation would encourage a more robust immune response (**Figure S4**). From these preliminary *in vivo* data, even though n-OVA@ZIF has marginally longer tissue residency times, we conclude that μ-OVA@ZIF is more biocompatible and may be more efficient at activating the immune system. Looking at both the *in vitro* and *in vivo* data, we decided that μ-OVA@ZIF was the preferred vaccine formulation and was therefore used in further experiments.

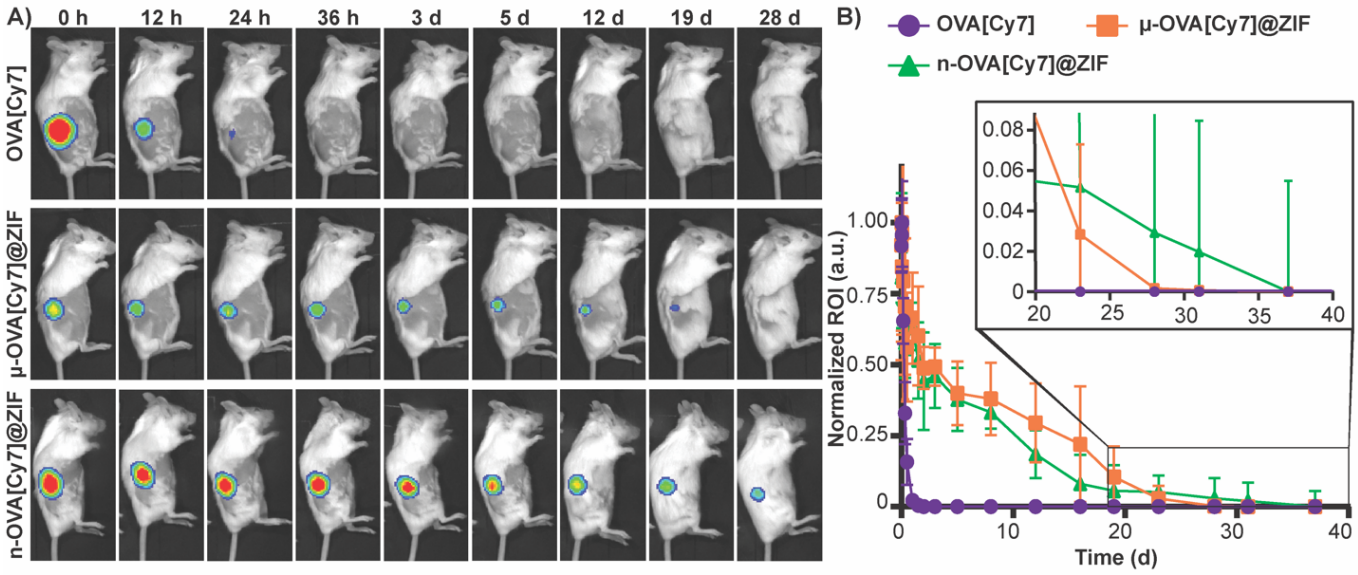

Figure 3. Evaluation of μ-OVA@ZIF and n-OVA@ZIF tissue residency. **A)** Representative images of Cy7 fluorescence in the right flank of mice subcutaneously injected with OVA[Cy7] (top), μ-OVA[Cy7]@ZIF (middle), and n-OVA[Cy7]@ZIF (bottom) **B)** Normalized Cy7 fluorescence from mice subcutaneously injected with OVA[Cy7], μ-OVA[Cy7]@ZIF, and n-OVA[Cy7]@ZIF (10 μg OVA[Cy7]) over the course of 38 days (n=4).

To qualitatively assess the degradation of ZIF-8 crystals, we injected 50 µL of µ-OVA@ZIF into BALB/c mice (n=2) (**Figure 3A**). 24 h, 48 h, 72 h, and 96 h post-vaccination, the mice were euthanized, and ZIF-8 crystals were extracted from the injection site as a white bio-aggregate clump (**Figure S5**). SEM images were taken of pristine and *ex vivo* ZIF-8 (**Figure 3B**). It is known that ZIF-8 degrades in both the presence of phosphates and albumin.[30] There was a definitive difference between pristine and *ex vivo* ZIF-8. After 24 h, some crystals maintained their rhombic dodecahedron shape, while others developed large cavitations. After 48 h, the crystals appeared to be majority amorphous in structure, and after 72 h, no obvious ZIF-8 crystals were seen in the SEM micrographs (**Figure 4B**). At 96 h post-injection, we could no longer find crystals with the naked eye, though fluorescence data clearly show the presence of antigen. We thus conclude that the OVA@ZIF persists as micro or nanoparticles too small to see with the unaided eye. It is worth noting that we were able to extract less material with every successive time point.

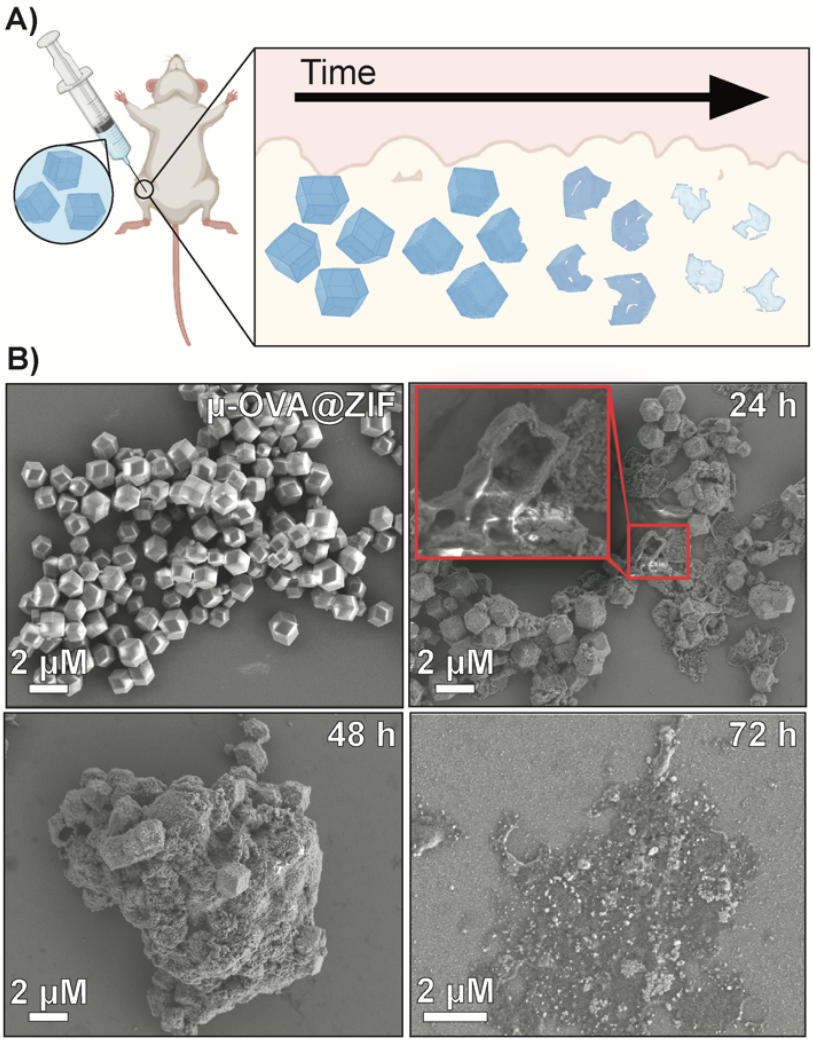

Figure 4. Degradation analysis of µ-OVA@ZIF post-injection. **A)** Schematic representation of the degradation of ZIF-8 crystals *in vivo.* **B)** SEM images of pristine µ-OVA@ZIF and the *ex vivo* extracts at 24 h, 48 h, and 72 h post-injection.

Adjuvanting of ZIF-8 and Germinal Center Development

The ability of ZIF-8 encapsulation to enhance the immune response against the model Ag, OVA, was evaluated *in vivo* by looking at the humoral response. Female BALB/c mice were injected with either three bolus injections of OVA or one dose of μ-OVA@ZIF (n=5). The single dose and two subsequent boosters delivered to each mouse contained 25 μg of OVA, so OVA 3× received thrice the amount of Ag. To simulate a booster dose injection schedule, mice were injected with OVA on days 0, 7, and 14. μ-OVA@ZIF was injected once on day 0. To investigate the long-term humoral immunity of single dose OVA@ZIF versus OVA 3×, total IgG was investigated from days 14 to 91 following the first administration of OVA@ZIF and OVA 3× (**Figure 5A**). Using ELISA, endpoint titer total IgG was determined using saline mice as the baseline. There was higher anti-OVA IgG in the serum of single dose μ-OVA@ZIF versus OVA 3× across all time points (**Figure 5B**).

GCs are crucial for successful immunization and immune memory, yielding antibody-producing plasma cells and long-lived memory B cells.[50] GCs form in secondary lymphoid tissues, such as lymph nodes, typically after 14-28 days following Ag exposure.[51] Ag-activated B cells enter the GC in what is known as the light zone (**LZ**) and undergo proliferation and rounds of somatic hypermutation (**SHM**), creating diverse clones of themselves. This diverse library of GC B cells will migrate to the dark zone (**DZ**) and begin affinity maturation where greater affinity antibodies are selected.[52, 53] GC B cells interact with follicular dendritic cells (**DC**) and T follicular helper cells (**Tfh**). Cells that "pass" the selection process will either differentiate into long-lived memory B cells or antibody-producing plasma cells or will return to the LZ and begin this process again. We observed higher populations of GC B cells on day 21 in the ILN of the μ-OVA@ZIF cohort compared to OVA 3× (**Figure 5C**). Memory B cells and plasma B cells arise from these GC, creating long-term immune memory and increased antibody production. We observe higher antibody titers in the μ-OVA@ZIF cohort until day 91, validating our hypothesis. Additionally, we observed higher IgG1+ GC B cells in the DLN of the μ-OVA@ZIF; this is indicative of class-switching recombination (**CSR**), a process where B cells begin to produce higher affinity antibodies (**Figure 5D)**. GC formation and CSR are two crucial benchmarks for assessing a vaccine's efficacy, as immune memory, long-term antibody production, and high-affinity antibodies are needed to maintain humoral immunity. The sustained release of the Ag by encapsulation in MOF provides a constant source of Ag, better equipping the immune system than three bolus injections of Ag. Additionally, hematoxylin and eosin (**H&E**) staining of tissue samples collected on day 21 show no significant sign of inflammation, tissue damage, or major morphological changes compared to saline (**Figure S6**).

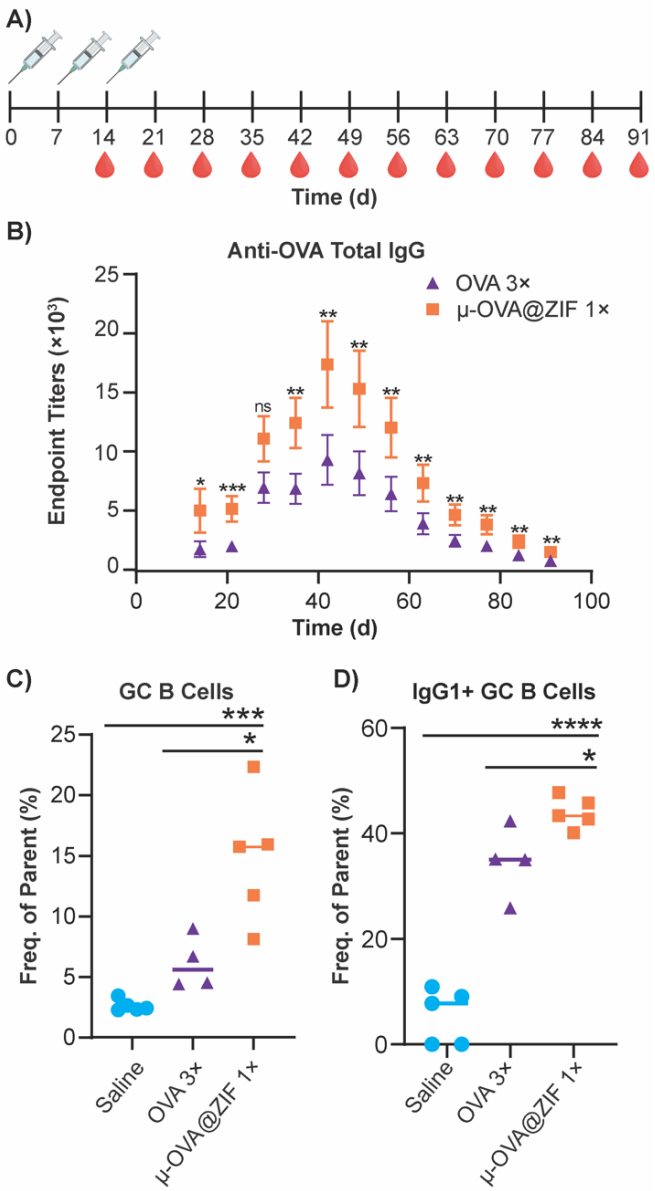

Figure 5: Humoral response of single dose μ-OVA@ZIF vs. OVA 3×. **A)** Scheme of vaccine and blood draw schedule for determining endpoint titers of Anti-OVA IgG. **B)** Endpoint titers of Anti-OVA IgG from mouse serum. **C)** Day 21 GC formation in the ILN of vaccinated mice. **D)** Percentage of IgG1+ GC B cells in the ILN. Statistical significance was determined by an unpaired T-test (P>0.05 is ns, P≤ 0.05 is *, P ≤ 0.01 is **, P ≤ 0.001, and P ≤ 0.0001 is ****).

Scalable Synthesis

Finally, to demonstrate our formulation's ease of preparation and scalability, we synthesized the μ-ZIF formulations under the same conditions previously mentioned—we increased the volumes and concentrations. We made 2 L of μ-ZIF (**Figures 6A and 6B**) and bovine serum albumin@ZIF (μ-BSA@ZIF) (**Figures 6A and 6B**). We encapsulated 500 mg of BSA[Cy-7] (250 μg/mL) in the 2 L ZIF-8 reaction. The reaction was left for 1 h on the benchtop (**Figure 6B**). The encapsulation

efficiency was 98.1% ±1.64, comparable to that of the 1 mL reaction of OVA@ZIF. Following a series of washes, the MOFs were dried under a vacuum, and the total weight of μ-ZIF was determined to be 15.9 g (**Figure 6c**). We used BSA in this case because Ag-grade OVA is expensive, and it would be wasteful to create this much OVA@ZIF as no lab could possibly use this much material. It is worth mentioning, however, that Ag doses given to mice are typically the same as those given to humans (between 5–50 μg per dose).[12, 54] This is the equivalent of 20,000 injections. Thus, this synthesis would prepare enough injections for a small town in an hour. PXRD patterns were obtained, and the sodalite crystallinity of both μ-BSA@ZIF and μ-ZIF was confirmed (**Figure 6D**)

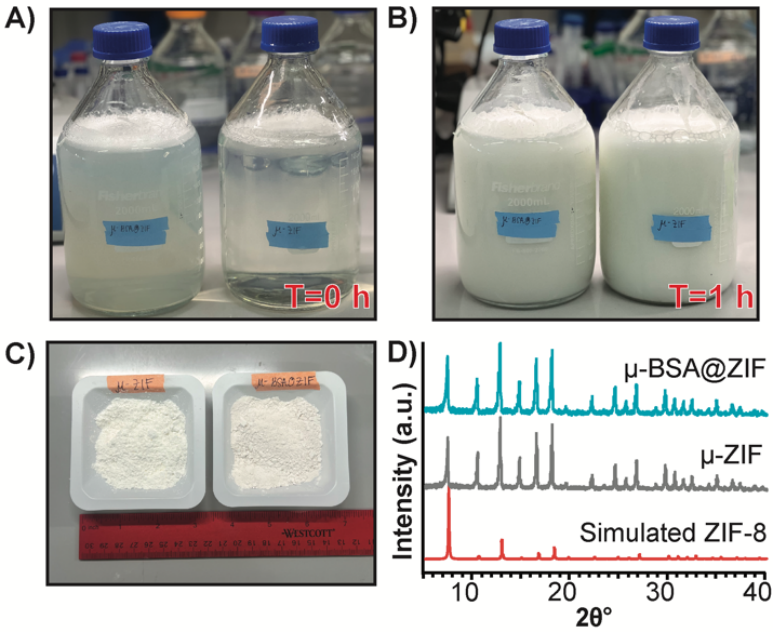

Figure 6: Scaled synthesis of μ-ZIF and μ-BSA[Cy7]@ZIF. **A)** Image of 2 L bottles (left: μ-BSA@ZIF, right: μ-ZIF) used for scaled-up ZIF synthesis at T=0 h and **B)** at T=1 h. **C)** 15.9 g of μ-ZIF powder (left) and 16.4 g μ-BSA[Cy7]@ZIF powder (right) from 2 L synthesis. **D)** PXRD patterns of μ-BSA[Cy7]@ZIF (top), μ-ZIF (middle), and simulated ZIF-8 (bottom) following scaled synthesis.

Conclusion

ZIF-8 has improved proteinaceous vaccine formulations by stabilizing and protecting proteins against thermal and enzymatic degradation. We have shown that ZIF-8 can also help the vaccine generate an enhanced immune response, significantly enough to overcome a three-series booster regimen. Regarding the humoral immune response, μ-OVA@ZIF demonstrates significantly higher serum antibody titers against OVA compared to three bolus Ag doses. Additionally, we've found that μ-OVA@ZIF has more GC B cells 21 days post the initial injection. Not only does ZIF-8 encapsulation allow us to generate a strong humoral immune response, but it also uses less Ag than the bolus injection regimen. ZIF-8 encapsulation can reduce the number of needle injections and the amount of expensive, precious biomaterial. Lastly, we determined that this synthesis is easily scaled to a 2 L reaction volume while maintaining the short reaction time (1 h) and high encapsulation efficiency of protein (98%).

Methods

Chemicals

Zinc acetate (**ZnOAc**), 2-methyl imidazole, sodium chloride, phosphate buffer saline (**PBS**) pH 7.4, Dulbecco's Modified Eagle Medium (**DMEM**), penicillin-streptomycin, L-glutamine, BSA, Ethylenediaminetetraacetic acid (**EDTA**), sodium bicarbonate (**$NaCO_3$**), dimethyl sulfoxide (**DMSO**), goat anti-mouse IgG (whole molecule)-alkaline phosphatase, magnesium chloride (**$MgCl_2$**), paraformaldehyde (**PFA**) *p*-nitrophenyl phosphate (**pNPP**), tween-20, polyvinyl pyrrolidine (**PVP**), diethanolamine, potassium phosphate dibasic, potassium phosphate monobasic, hydrochloric acid, and sodium hydroxide were purchased from Sigma Aldrich (St. Louis, MO, USA) or Thermofisher Scientific (Waltham, MA, USA) and used without further modification. FBessence was purchased from VWR (Radnor, PA, USA). LDH assay, cell staining buffer (**CSB**), Zombie Red, Zombie UV, anti-mouse CD19 Alex Fluor 700 (**AF700**), anti-mouse IgG1 phyco-erythrin (**PE**), anti-mouse CD95 allophycocyanin (**APC**), and anti-mouse GL7 Alexa Fluor 488 (**AF488**)were purchased from Biolegend (San Diego, CA, USA). Vaccine-grade, endotoxin-free OVA was purchased from Invitrogen (Waltham, MA, USA) and Worthington Biochemical (Lakewood, NJ, USA). Bradford protein assay was purchased from BioRad Laboratories (Hercules, CA, USA). Non-fluorescent mouse diet was purchased from Lab Supply (Northlake, TX, USA). Cyanine 7-NHS (**Cy7-NHS**) was purchased from Lumiprobe (Cockeysville, MD, USA) and synthesized (**Figure S8-19**).

Instruments

SEM micrographs were taken on Zeiss Supra 40. PXRD patterns were obtained from Rigaku SmartLab X-ray diffractometer. Absorbance and fluorescence spectra were obtained on Biotek Synergy H4 Hybrid microplate reader. Thermofisher Scientific Sorvall Legend Micro17, Thermofisher Scientific Sorvall Lynx 4000, and Beckman Coulter Allegra X-14R centrifuges were used for obtaining cell and ZIF-8 pellets. CLSM images were taken on Olympus FV3000 RS microscope. Flow cytometry data were acquired on a BD LSRFortessa. Cell counting was carried out on a Thermo Countess II. Live animal imaging was performed on an IVIS Lumina III. Paraffin embedding was done on Histo-Core ARCADIA. Embedded tissues were processed with a Leica RM22335 microtome. H&E images were obtained on VS120 virtual slide microscope. Ultrapure water was filtered in lab with the ELGA PURELAB flex 2 system.

Animals and ethics

Female BALB/c mice (4-6 weeks) were purchased from Charles Rivers Laboratories (Wilmington, MA, USA). *In vivo* experiments were approved by the University of Texas at Dallas Institutional Animal Care and Use Committee. This work was diligently carried out in accordance to protocol #19-06.

ZIF-8 synthesis

1M ZnOAc and 3M mIM stocks were made in sterile water (filtered and autoclaved). The final stock solutions were filtered through a 0.22 μM syringe filter. All microscale reactions took place at a final volume of 1 mL. For the nano-sized MOFs, sterile water, ovalbumin (150 μg/mL in water), 2560 mM mIM, and 80 mM ZnOAc were added sequentially, vortexing after each addition. For the micro-sized MOFs, sterile water, OVA (150 μg/mL), 640 mM mIM, and 40 mM ZnOAc were added sequentially, vortexing after each addition. The reaction vial was left for 1 h

at RT. The resulting crystals were washed 3× by centrifuging at 17,000 ×*g* for 5 min. The supernatant was removed, and the pellet was resuspended in 1 mL of sterile water.

Fluorescent labeling of protein

For OVA[Cy7], 10 mg/mL OVA was dissolved in 1 mL of 0.1 M $NaCO_3$ (pH 8.3). 63 µL of Cy7-NHS in DMSO dye solution was added to the OVA solution and vortexed well. The protein-dye solution was incubated overnight on a rotisserie at 4 ºC. The solution was washed with water in a 10 kDa protein concentrator at 4000 ×*g* for 10 min until the filtrate was clear. The concentration of protein was determined through Bradford protein assay.

For BSA[Cy7] 1 g of BSA dissolved in 0.1 M $NaCO_3$ (pH 8.3). 1 mg of synthesized Cy7-NHS was dissolved in 200 µL of DMSO. The Cy7-NHS was added to the protein solution and vortexed well. The protein-dye solution was incubated overnight on a rotisserie at 4 ºC. The solution was washed with water in a 10 kDa protein concentrator at 4000 ×*g* for 10 min until the filtrate was clear, indicating that the free Cy7 dye was removed. The concentration of protein was determined through Bradford Protein Assay.

Cell culture

RAW 264.7 murine macrophages were cultured in DMEM supplemented with 1% L-Glutamine, 2% penicillin-streptomycin, and 10% FBessence in a 75 cm^2 culture flask. Cells were grown at 37 °C with 5% CO_2. Cells were passaged at 80-95% confluency by removing media, rinsing with 0.1M PBS, followed by an additional 0.1 M PBS, and detaching cells with a cell scraper. The cell solution was centrifuged at 300 ×g for 2 min.

Cytotoxicity

The night before, 1 × 10^5 viable RAW 264.7 cells were seeded in a 96-well plate in supplemented DMEM. Old media was aspirated. OVA, µ- and n-OVA@ZIF samples were diluted in complete DMEM and added to wells at a final volume of 100 µL. The cells were incubated with samples for 4 h at 37°C with 5% CO_2. Following the protocol from the LDH assay kit, 20 µL of lysis buffer was added to the high control and left to incubate for an additional 20 min at 37 °C with 5% CO_2. Then, 100 µL of the working solution was added to each well and left to incubate in the dark for 20 min. 50 µL of stop solution was added, and the absorbance was read at 490 nm. Cell viability was determined through the following equation: $1 - \left(\left(\frac{\text{abs.of test substance} - \text{abs. low control}}{\text{abs. high control} - \text{abs. low control}}\right) \times 100\right)$.

***In vitro* uptake**

For uptake studies, 1 × 10^6 cells were added to a 24-well plate with 2 µg OVA[Cy7], 8 µL of µ- and n-OVA[Cy7]@ZIF (2 µg OVA). The cells were incubated with samples for 4 h at 37 °C with 5% CO_2. The cells were washed 3× with 0.5 M EDTA and 3× with PBS. Cells were stained with a 1:2000 Zombie Red solution in PBS for 20 min on ice and in the dark. Cells were centrifuged and resuspended in CSB (0.1 M PBS, 5% FBS, 0.5 mM EDTA, and 2 mM NaN_3). Flow cytometry analysis was performed on a BD LSRFortessa flow cytometer, and 100,000 events were recorded. Raw data were processed and analyzed using FlowJo software. Dead cells were gated out by selecting the negative Zombie Red population, and Cy7 positive cells were assumed to have uptake OVA. The Histogram overlay was normalized to mode.

Tissue residency
12 female BALB/c (n=4) mice were fed a non-fluorescent diet for at least 48 h before the start of the experiment. The day before vaccination, mice were depilated with Nair hair remover on the side of the injection. Mice were anesthetized with isoflurane before injections or imaging. Baseline images of each mouse were obtained before the injection of the sample. OVA[Cy7], μ-OVA[Cy7]@ZIF, and n-OVA[Cy7]@ZIF (10 μg OVA per dose) were injected subcutaneously with the sample into the right flank of each mouse. Mice were imaged at t=0 h, 0.5 h, 1 h, 2 h, 4 h, 8 h, 24 h, 36 h, 2 d, 3 d, 5 d, 8 d, 12 d, 16 d, 19 d, 23 d, 28 d, 31 d, and 37 d. Data were normalized using GraphPad Prism.

***Ex vivo* degradation**
100 μL of μ-OVA@ZIF in 0.1 M saline were injected into both flanks (to increase the chance of retrieving the sample) of female BALB/c mice (n=2). Mice were euthanized through cervical dislocation, and samples were removed from the subcutaneous layer at 24, 48, 72, and 96 h (no sample was found at 96 h). Samples were washed 3× with water.

In *vivo* antibody production
Female BALB/c mice (n=5) were vaccinated subcutaneously with three doses of 100 μL 0.1 M saline and 100 μL OVA (75 μg OVA total) on days 0, 7, and 14. Additionally, one dose of μ-OVA@ZIF (25 μg OVA) on day 0. Mice were anesthetized with isoflurane, and blood was drawn weekly from day 14 until day 98. The serum was isolated by centrifuging blood samples at 1200 ×g for 10 min to remove red blood cells. Serum was stored at -20°C until further use.

Endpoint Titer Anti-OVA IgG ELISA
96-well Nunc titer plate was coated the night before with 100 μL 1 μg/mL OVA in coating buffer (0.05 M $NaCO_3$ buffer pH 9.6). The plate was left to incubate overnight at 4 °C. Plate was washed 4× with 300 μL of wash buffer (0.1 M PBS 0.05% w/v tween-20 pH 7.4). The plate was blocked with 200 μL of assay diluent (1% BSA in wash buffer) for 1 h at 37°C. The plate was washed 5× with wash buffer, and 100 μL of serially diluted serum (100×-3200×) in assay diluent was added to each well. The plate was incubated at 37 °C for 1.5 h. The plate was subsequently washed 4× with wash buffer, followed by the addition of 100 μL of (1:2000) alkaline phosphatase-conjugated goat anti-mouse IgG in conjugate buffer (0.02 g of PVP/mL assay diluent). The plate was incubated at 37 °C for 1 h. The plate was incubated at 37°C for 1 h. The plate was washed 4× with wash buffer. 100 μL of 1 mg/mL pNPP in substrate buffer (1 M diethanolamine buffer, 0.5 mM $MgCl_2$ pH 9.8) was added to the plate and left in the dark to incubate for 15 min or until color developed. Absorbance was read at 450 nm at 15 and 30 min. The endpoint titer was determined by plotting the dilution factor against 450 nm absorbance. The logarithmic curve was fit, and the endpoint titer was determined by the intersection of logarithmic fit to the average baseline (saline).

***In vivo* GC study**
Female BALB/c mice (n=5) were vaccinated subcutaneously with three doses of 100 μL 0.1 M saline and 100 μL OVA (75 μg OVA total) on days 0, 7, and 14. Additionally, one dose of μ-OVA@ZIF (25 μg OVA) on day 0. Mice were anesthetized before vaccination. On day 21, mice were euthanized via cervical dislocation, and the ILN was extracted along with other major organs (heart, lung, liver, and kidney) for H&E staining. A single-cell suspension was obtained by

carefully passing cells through a 100 µM cell strainer. Cells were washed 1× with 0.1 M PBS, resuspended in 1 mL of 0.1 M PBS, and counted using Trypan Blue to determine live/dead cells. Cells were stained with Zombie UV (1:2000) in 0.1 M PBS for 30 min on ice in the dark. Subsequently, the antibody cocktail (anti-mouse CD19 AF700, anti-mouse IgG1 PE, anti-mouse CD95 APC, and anti-mouse GL7 AF 488 in CSB) was added to the cells. The cells were left to stain for 30 minutes on ice in the dark. Cells were washed 3× with FACS buffer. Flow cytometry analysis was carried out on a BD LSRFortessa flow cytometer. Raw data were processed and analyzed using FlowJo software.

H&E

Organs were incubated in 4% PFA for 48 h at ambient T on a shaker. Tissues were washed 3× with 0.1 M PBS, placed into tissue cassettes, and then into 70% ethanol. The organs were embedded in paraffin wax. Each organ was sectioned into 5 µm section using a rotary microtome. The sections were collected and stained with H&E for pathological analysis.

Scaled ZIF-8 Synthesis

2 L of µ-ZIF was synthesized by adding 640 mM mIM, 40 mM ZnOAc, bringing the final volume to 2 L with MilliQ water. 2 L of µ-BSA[Cy7]@ZIF was synthesized by 640 mM mIM, 40 mM ZnOAc, 500 mg of BSA[Cy7]. The reaction bottles were vigorously shaken after adding the precursors and left to incubate for 1 h at ambient T. Solutions were transferred to 1 L centrifuge bottles and centrifuged for 30 min at 17,000 ×g. The supernatant was discarded, and ZIF was resuspended in 200 mL of water, transferred to 50 mL disposable centrifuge tubes, and washed 2× with water. Tubes were then placed under a vacuum for drying.

Author Contributions

Conceptualization: J.J.G. Methodology: R.N.E., O.R.B., Y.H.W., S. Kumari, F.C.H., Investigation: R.N.E., O.R.B., Y.H.W., S. Kumari, I.T., O.T., T.S.H., F.C.H., A.J., S. Koirala, N.T., N.M.A. Manuscript preparation: R.N.E. and J.J.G.

Conflicts of Interest

The authors declare no competing interests.

Acknowledgments

We thank Dr. Rockford Draper (University of Texas at Dallas) for the gift of RAW 264.7 cells. Additionally, we would like to thank the University of Texas at Dallas lab animal resource center and its staff for their assistance in the care and maintenance of animals. J.J.G. would like to thank the National Science Foundation *(DMR- 2003534) and the Welch Foundation (AT-198920190330) for their support.*

References

(1) Henderson, D. A. Edward Jenner's vaccine. *Public Health Rep* **1997**, *112* (2), 116-121. From NLM.
(2) Plotkin, S. A. Vaccines: past, present and future. *Nature Medicine* **2005**, *11* (4), S5-S11. DOI: 10.1038/nm1209.

(3) Pezzotti, P.; Bellino, S.; Prestinaci, F.; Iacchini, S.; Lucaroni, F.; Camoni, L.; Barbieri, M. M.; Ricciardi, W.; Stefanelli, P.; Rezza, G. The impact of immunization programs on 10 vaccine preventable diseases in Italy: 1900–2015. *Vaccine* **2018**, *36* (11), 1435-1443. DOI: https://doi.org/10.1016/j.vaccine.2018.01.065.
(4) Moyle, P. M.; Toth, I. Modern Subunit Vaccines: Development, Components, and Research Opportunities. *ChemMedChem* **2013**, *8* (3), 360-376. DOI: https://doi.org/10.1002/cmdc.201200487.
(5) Vartak, A.; Sucheck, S. J. Recent Advances in Subunit Vaccine Carriers. *Vaccines (Basel)* **2016**, *4* (2). DOI: 10.3390/vaccines4020012 From NLM.
(6) Hansson, M.; Nygren, P.-A. k.; Sta˚hl, S. Design and production of recombinant subunit vaccines. *Biotechnology and Applied Biochemistry* **2000**, *32* (2), 95-107. DOI: https://doi.org/10.1042/BA20000034.
(7) Welch, R. P.; Lee, H.; Luzuriaga, M. A.; Brohlin, O. R.; Gassensmith, J. J. Protein–Polymer Delivery: Chemistry from the Cold Chain to the Clinic. *Bioconjugate Chemistry* **2018**, *29* (9), 2867-2883. DOI: 10.1021/acs.bioconjchem.8b00483.
(8) Riccò, R.; Liang, W.; Li, S.; Gassensmith, J. J.; Caruso, F.; Doonan, C.; Falcaro, P. Metal–Organic Frameworks for Cell and Virus Biology: A Perspective. *ACS Nano* **2018**, *12* (1), 13-23. DOI: 10.1021/acsnano.7b08056.
(9) Matthias, D. M.; Robertson, J.; Garrison, M. M.; Newland, S.; Nelson, C. Freezing temperatures in the vaccine cold chain: A systematic literature review. *Vaccine* **2007**, *25* (20), 3980-3986. DOI: https://doi.org/10.1016/j.vaccine.2007.02.052.
(10) Heidary, M.; Kaviar, V. H.; Shirani, M.; Ghanavati, R.; Motahar, M.; Sholeh, M.; Ghahramanpour, H.; Khoshnood, S. A comprehensive review of the protein subunit vaccines against COVID-19. *Frontiers in microbiology* **2022**, *13*, 927306.
(11) Poorolajal, J.; Mahmoodi, M.; Majdzadeh, R.; Nasseri-Moghaddam, S.; Haghdoost, A.; Fotouhi, A. Long-term protection provided by hepatitis B vaccine and need for booster dose: A meta-analysis. *Vaccine* **2010**, *28* (3), 623-631. DOI: https://doi.org/10.1016/j.vaccine.2009.10.068.
(12) Manoff, S. B.; George, S. L.; Bett, A. J.; Yelmene, M. L.; Dhanasekaran, G.; Eggemeyer, L.; Sausser, M. L.; Dubey, S. A.; Casimiro, D. R.; Clements, D. E.; et al. Preclinical and clinical development of a dengue recombinant subunit vaccine. *Vaccine* **2015**, *33* (50), 7126-7134. DOI: https://doi.org/10.1016/j.vaccine.2015.09.101.
(13) Liao, Y.; Chen, Y.; Chen, B.; Liang, Z.; Hu, X.; Xing, B.; Yang, J.; Zheng, Q.; Hua, Q.; Yan, C. Safety and immunogenicity of heterologous recombinant protein subunit vaccine (ZF2001) booster against COVID-19 at 3–9-month intervals following two-dose inactivated vaccine (CoronaVac). *Frontiers in Immunology* **2022**, *13*.
(14) Racine, É.; Gilca, V.; Amini, R.; Tunis, M.; Ismail, S.; Sauvageau, C. A systematic literature review of the recombinant subunit herpes zoster vaccine use in immunocompromised 18–49 year old patients. *Vaccine* **2020**, *38* (40), 6205-6214. DOI: https://doi.org/10.1016/j.vaccine.2020.07.049.
(15) Bridges, C. B.; Watson, T. L.; Nelson, N. P.; Chavez-Torres, M.; Fineis, P.; Ntiri-Reid, B.; Wake, E.; Leahy, J. M.; Kurian, A. K.; Hall, M. A. K.; et al. Challenges with hepatitis B vaccination of high risk adults - A pilot program. *Vaccine* **2019**, *37* (35), 5111-5120. DOI: 10.1016/j.vaccine.2019.05.089 From NLM.

(16) Taddio, A.; Ipp, M.; Thivakaran, S.; Jamal, A.; Parikh, C.; Smart, S.; Sovran, J.; Stephens, D.; Katz, J. Survey of the prevalence of immunization non-compliance due to needle fears in children and adults. *Vaccine* **2012**, *30* (32), 4807-4812. DOI: https://doi.org/10.1016/j.vaccine.2012.05.011.
(17) Nelson, J. C.; Bittner, R. C. L.; Bounds, L.; Zhao, S.; Baggs, J.; Donahue, J. G.; Hambidge, S. J.; Jacobsen, S. J.; Klein, N. P.; Naleway, A. L.; et al. Compliance With Multiple-Dose Vaccine Schedules Among Older Children, Adolescents, and Adults: Results From a Vaccine Safety Datalink Study. *American Journal of Public Health* **2009**, *99* (S2), S389-S397. DOI: 10.2105/ajph.2008.151332.
(18) Ventola, C. L. Immunization in the United States: Recommendations, Barriers, and Measures to Improve Compliance: Part 1: Childhood Vaccinations. *P t* **2016**, *41* (7), 426-436. From NLM.
(19) Kurosky, S. K.; Davis, K. L.; Krishnarajah, G. Completion and compliance of childhood vaccinations in the United States. *Vaccine* **2016**, *34* (3), 387-394. DOI: https://doi.org/10.1016/j.vaccine.2015.11.011.
(20) Taddio, A.; McMurtry, C. M.; Logeman, C.; Gudzak, V.; de Boer, A.; Constantin, K.; Lee, S.; Moline, R.; Uleryk, E.; Chera, T.; et al. Prevalence of pain and fear as barriers to vaccination in children – Systematic review and meta-analysis. *Vaccine* **2022**, *40* (52), 7526-7537. DOI: https://doi.org/10.1016/j.vaccine.2022.10.026.
(21) Brohlin, O. R.; Ehrman, R. N.; Herbert, F. C.; Wijesundara, Y. H.; Raja, A.; Shahrivarkevishahi, A.; Diwakara, S. D.; Smaldone, R. A.; Gassensmith, J. J. Zeolitic Imidazolate Framework Nanoencapsulation of CpG for Stabilization and Enhancement of Immunoadjuvancy. *ACS Applied Nano Materials* **2022**, *5* (10), 13697-13704. DOI: 10.1021/acsanm.1c03555.
(22) Herbert, F. C.; Abeyrathna, S. S.; Abeyrathna, N. S.; Wijesundara, Y. H.; Brohlin, O. R.; Carraro, F.; Amenitsch, H.; Falcaro, P.; Luzuriaga, M. A.; Durand-Silva, A.; et al. Stabilization of supramolecular membrane protein–lipid bilayer assemblies through immobilization in a crystalline exoskeleton. *Nature Communications* **2021**, *12* (1), 2202. DOI: 10.1038/s41467-021-22285-y.
(23) Kumari, S.; Wijesundara, Y. H.; Howlett, T. S.; Waliullah, M.; Herbert, F. C.; Raja, A.; Trashi, I.; Bernal, R. A.; Gassensmith, J. J. Biolistic delivery of liposomes protected in metal-organic frameworks. *Proceedings of the National Academy of Sciences* **2023**, *120* (11), e2218247120. DOI: 10.1073/pnas.2218247120 (acccessed 2023/06/12).
(24) Liang, W.; Wied, P.; Carraro, F.; Sumby, C. J.; Nidetzky, B.; Tsung, C.-K.; Falcaro, P.; Doonan, C. J. Metal–Organic Framework-Based Enzyme Biocomposites. *Chemical Reviews* **2021**, *121* (3), 1077-1129. DOI: 10.1021/acs.chemrev.0c01029.
(25) Liang, K.; Ricco, R.; Doherty, C. M.; Styles, M. J.; Bell, S.; Kirby, N.; Mudie, S.; Haylock, D.; Hill, A. J.; Doonan, C. J.; et al. Biomimetic mineralization of metal-organic frameworks as protective coatings for biomacromolecules. *Nature Communications* **2015**, *6* (1), 7240. DOI: 10.1038/ncomms8240.
(26) Yang, J.; Yang, Y.-W. Metal–Organic Frameworks for Biomedical Applications. *Small* **2020**, *16* (10), 1906846, https://doi.org/10.1002/smll.201906846. DOI: https://doi.org/10.1002/smll.201906846 (acccessed 2023/06/12).
(27) Luzuriaga, M. A.; Herbert, F. C.; Brohlin, O. R.; Gadhvi, J.; Howlett, T.; Shahrivarkevishahi, A.; Wijesundara, Y. H.; Venkitapathi, S.; Veera, K.; Ehrman, R.; et al. Metal–Organic Framework

Encapsulated Whole-Cell Vaccines Enhance Humoral Immunity against Bacterial Infection. *ACS Nano* **2021**, *15* (11), 17426-17438. DOI: 10.1021/acsnano.1c03092.
(28) Luzuriaga, M. A.; Welch, R. P.; Dharmarwardana, M.; Benjamin, C. E.; Li, S.; Shahrivarkevishahi, A.; Popal, S.; Tuong, L. H.; Creswell, C. T.; Gassensmith, J. J. Enhanced Stability and Controlled Delivery of MOF-Encapsulated Vaccines and Their Immunogenic Response In Vivo. *ACS Applied Materials & Interfaces* **2019**, *11* (10), 9740-9746. DOI: 10.1021/acsami.8b20504.
(29) Wijesundara, Y. H.; Herbert, F. C.; Trashi, O.; Trashi, I.; Brohlin, O. R.; Kumari, S.; Howlett, T.; Benjamin, C. E.; Shahrivarkevishahi, A.; Diwakara, S. D.; et al. Carrier gas triggered controlled biolistic delivery of DNA and protein therapeutics from metal–organic frameworks. *Chemical Science* **2022**, *13* (46), 13803-13814, 10.1039/D2SC04982A. DOI: 10.1039/D2SC04982A.
(30) Luzuriaga, M. A.; Benjamin, C. E.; Gaertner, M. W.; Lee, H.; Herbert, F. C.; Mallick, S.; Gassensmith, J. J. ZIF-8 degrades in cell media, serum, and some—but not all—common laboratory buffers. *Supramolecular Chemistry* **2019**, *31* (8), 485-490. DOI: 10.1080/10610278.2019.1616089.
(31) Cheng, C.; Li, C.; Zhu, X.; Han, W.; Li, J.; Lv, Y. Doxorubicin-loaded Fe3O4-ZIF-8 nano-composites for hepatocellular carcinoma therapy. *Journal of Biomaterials Applications* **2019**, *33* (10), 1373-1381. DOI: 10.1177/0885328219836540.
(32) Teng, Z.; Hou, F.; Bai, M.; Li, J.; Wang, J.; Wu, J.; Ru, J.; Ren, M.; Sun, S.; Guo, H. Bio-mineralization of virus-like particles by metal–organic framework nanoparticles enhances the thermostability and immune responses of the vaccines. *Journal of Materials Chemistry B* **2022**, *10* (15), 2853-2864, 10.1039/D1TB02719K. DOI: 10.1039/D1TB02719K.
(33) Luzuriaga, M. A.; Shahrivarkevishahi, A.; Herbert, F. C.; Wijesundara, Y. H.; Gassensmith, J. J. Biomaterials and nanomaterials for sustained release vaccine delivery. *WIREs Nanomedicine and Nanobiotechnology* **2021**, *13* (6), e1735. DOI: https://doi.org/10.1002/wnan.1735.
(34) Tam, H. H.; Melo, M. B.; Kang, M.; Pelet, J. M.; Ruda, V. M.; Foley, M. H.; Hu, J. K.; Kumari, S.; Crampton, J.; Baldeon, A. D.; et al. Sustained antigen availability during germinal center initiation enhances antibody responses to vaccination. *Proceedings of the National Academy of Sciences* **2016**, *113* (43), E6639-E6648. DOI: doi:10.1073/pnas.1606050113.
(35) Cirelli, K. M.; Crotty, S. Germinal center enhancement by extended antigen availability. *Curr Opin Immunol* **2017**, *47*, 64-69. DOI: 10.1016/j.coi.2017.06.008 From NLM.
(36) Boopathy, A. V.; Mandal, A.; Kulp, D. W.; Menis, S.; Bennett, N. R.; Watkins, H. C.; Wang, W.; Martin, J. T.; Thai, N. T.; He, Y.; et al. Enhancing humoral immunity via sustained-release implantable microneedle patch vaccination. *Proceedings of the National Academy of Sciences* **2019**, *116* (33), 16473-16478. DOI: doi:10.1073/pnas.1902179116.
(37) Roth, G. A.; Gale, E. C.; Alcántara-Hernández, M.; Luo, W.; Axpe, E.; Verma, R.; Yin, Q.; Yu, A. C.; Lopez Hernandez, H.; Maikawa, C. L.; et al. Injectable Hydrogels for Sustained Codelivery of Subunit Vaccines Enhance Humoral Immunity. *ACS Central Science* **2020**, *6* (10), 1800-1812. DOI: 10.1021/acscentsci.0c00732.
(38) Cirelli, K. M.; Carnathan, D. G.; Nogal, B.; Martin, J. T.; Rodriguez, O. L.; Upadhyay, A. A.; Enemuo, C. A.; Gebru, E. H.; Choe, Y.; Viviano, F.; et al. Slow Delivery Immunization Enhances HIV Neutralizing Antibody and Germinal Center Responses via Modulation of Immunodominance. *Cell* **2019**, *177* (5), 1153-1171.e1128. DOI: 10.1016/j.cell.2019.04.012 From NLM.

(39) Ou, B. S.; Saouaf, O. M.; Baillet, J.; Appel, E. A. Sustained delivery approaches to improving adaptive immune responses. *Advanced Drug Delivery Reviews* **2022**, *187*, 114401. DOI: https://doi.org/10.1016/j.addr.2022.114401.
(40) Kräutler, N. J.; Suan, D.; Butt, D.; Bourne, K.; Hermes, J. R.; Chan, T. D.; Sundling, C.; Kaplan, W.; Schofield, P.; Jackson, J.; et al. Differentiation of germinal center B cells into plasma cells is initiated by high-affinity antigen and completed by Tfh cells. *J Exp Med* **2017**, *214* (5), 1259-1267. DOI: 10.1084/jem.20161533 From NLM.
(41) Kumari, S.; Howlett, T. S.; Ehrman, R. N.; Koirala, S.; Trashi, O.; Trashi, I.; Wijesundara, Y. H.; Gassensmith, J. J. In vivo biocompatibility of ZIF-8 for slow release via intranasal administration. *Chemical Science* **2023**, *14* (21), 5774-5782, 10.1039/D3SC00500C. DOI: 10.1039/D3SC00500C.
(42) Hoop, M.; Walde, C. F.; Riccò, R.; Mushtaq, F.; Terzopoulou, A.; Chen, X.-Z.; deMello, A. J.; Doonan, C. J.; Falcaro, P.; Nelson, B. J.; et al. Biocompatibility characteristics of the metal organic framework ZIF-8 for therapeutical applications. *Applied Materials Today* **2018**, *11*, 13-21. DOI: https://doi.org/10.1016/j.apmt.2017.12.014.
(43) Lin, J.; Huang, L.; Ou, H.; Chen, A.; Xiang, R.; Liu, Z. Effects of ZIF-8 MOFs on structure and function of blood components. *RSC Advances* **2021**, *11* (35), 21414-21425, 10.1039/D1RA02873A. DOI: 10.1039/D1RA02873A.
(44) Kool, M.; Fierens, K.; Lambrecht, B. N. Alum adjuvant: some of the tricks of the oldest adjuvant. *Journal of Medical Microbiology* **2012**, *61* (7), 927-934. DOI: https://doi.org/10.1099/jmm.0.038943-0.
(45) HogenEsch, H. Mechanism of Immunopotentiation and Safety of Aluminum Adjuvants. *Frontiers in Immunology* **2013**, *3*, Review. DOI: 10.3389/fimmu.2012.00406.
(46) Portuondo, D. L.; Batista-Duharte, A.; Ferreira, L. S.; de Andrade, C. R.; Quinello, C.; Téllez-Martínez, D.; de Aguiar Loesch, M. L.; Carlos, I. Z. Comparative efficacy and toxicity of two vaccine candidates against Sporothrix schenckii using either Montanide™ Pet Gel A or aluminum hydroxide adjuvants in mice. *Vaccine* **2017**, *35* (34), 4430-4436. DOI: https://doi.org/10.1016/j.vaccine.2017.05.046.
(47) Goto, N.; Kato, H.; Maeyama, J.-i.; Eto, K.; Yoshihara, S. Studies on the toxicities of aluminium hydroxide and calcium phosphate as immunological adjuvants for vaccines. *Vaccine* **1993**, *11* (9), 914-918. DOI: https://doi.org/10.1016/0264-410X(93)90377-A.
(48) Andorko, J. I.; Hess, K. L.; Jewell, C. M. Harnessing Biomaterials to Engineer the Lymph Node Microenvironment for Immunity or Tolerance. *The AAPS Journal* **2015**, *17* (2), 323-338. DOI: 10.1208/s12248-014-9708-2.
(49) Moyer, T. J.; Zmolek, A. C.; Irvine, D. J. Beyond antigens and adjuvants: formulating future vaccines. *The Journal of Clinical Investigation* **2016**, *126* (3), 799-808. DOI: 10.1172/JCI81083.
(50) Hägglöf, T.; Cipolla, M.; Loewe, M.; Chen, S. T.; Mesin, L.; Hartweger, H.; ElTanbouly, M. A.; Cho, A.; Gazumyan, A.; Ramos, V.; et al. Continuous germinal center invasion contributes to the diversity of the immune response. *Cell* **2022**. DOI: https://doi.org/10.1016/j.cell.2022.11.032.
(51) Lee, J. H.; Sutton, H. J.; Cottrell, C. A.; Phung, I.; Ozorowski, G.; Sewall, L. M.; Nedellec, R.; Nakao, C.; Silva, M.; Richey, S. T.; et al. Long-primed germinal centres with enduring affinity maturation and clonal migration. *Nature* **2022**, *609* (7929), 998-1004. DOI: 10.1038/s41586-022-05216-9.
(52) De Silva, N. S.; Klein, U. Dynamics of B cells in germinal centres. *Nature Reviews Immunology* **2015**, *15* (3), 137-148. DOI: 10.1038/nri3804.

(53) Victora, G. D.; Nussenzweig, M. C. Germinal centers. *Annu Rev Immunol* **2012**, *30*, 429-457. DOI: 10.1146/annurev-immunol-020711-075032 From NLM.
(54) Heidary, M.; Kaviar, V. H.; Shirani, M.; Ghanavati, R.; Motahar, M.; Sholeh, M.; Ghahramanpour, H.; Khoshnood, S. A Comprehensive Review of the Protein Subunit Vaccines Against COVID-19. *Front Microbiol* **2022**, *13*, 927306. DOI: 10.3389/fmicb.2022.927306 From NLM.